Linear and Nonlinear Properties of Geodesic Acoustic Mode and Beta-induced Alfvén Eigenmode

H. S. Zhang 1,2), L. Chen 2,3), I. Holod 2), Z. Lin 2), Z. Qiu 3), X. Wang 2,3), Y. Xiao 2), W. L. Zhang 2,4)

1) Fusion Simulation Center, Peking University, Beijing 100871, China
2) Department of Physics and Astronomy, University of California, Irvine, CA92697, USA
3) Institute for Fusion Theory and Simulation, Zhejiang University, Hangzhou 310027, China
4) Department of Modern Physics, University of Science and Technology of China, Hefei 230026, China

E-mail contact: zhang.huasen@gmail.com

Abstract. Global gyrokinetic toroidal code (GTC) is used to study the low-frequency modes in tokamaks including geodesic acoustic mode (GAM) and beta-induced Alfvén eigenmode (BAE). GAM and BAE have the same frequency due to the geodesic curvature and thermal particle compressibility in toroidal plasmas. Important new insights include: the collisionless damping rate of the GAM is greatly enhanced by trapped electrons in the high-q region of tokamak (q is the safety factor) due to the resonance of the GAM oscillation with the trapped electron bounce motion; nonlinear self-interactions of the GAM cannot efficiently generate the second harmonic due to a cancellation between the perpendicular convective nonlinearity and the parallel nonlinearity for the long wavelength GAM; the BAE is excited by antenna and energetic particles, the non-perturbative contributions by energetic particles modify the mode structure and reduce the frequency of the stable eigenmodes relative to the ideal magnetohydrodynamic (MHD) theory.

1. Introduction

Geodesic acoustic mode (GAM)[1] and beta-induced Alfvén eigenmode (BAE)[2] have been widely observed in tokamak experiments[3, 4]. They have the same frequency, which is on the order of ion transit frequency, and can be damped through ion Landau damping. GAM is an electrostatic mode and is often observed at the edge of the tokamak, while BAE is an electromagnetic mode. GAM and BAE can degenerate at the mode rational surface. In this work, we use the global gyrokinetic toroidal code (GTC)[5, 6] to study the linear and nonlinear properties of GAM and the excitation of BAE. In the GAM collisionless damping study[7], it is found that the GAM damping rate is greatly enhanced by the trapped electrons through a resonance of the bounce motion with the GAM oscillation. This resonance is clearly verified by the structure of the perturbed electron distribution function in the phase space. In the GAM nonlinear self-interaction study[8], GTC simulations without the parallel nonlinearity find the generation of the second harmonic ($\omega = 2\omega_{GAM}$) quasimodes when the GAM amplitude increases to the experimentally-relevant level. The generation of the second harmonic of the GAM is much weaker when the parallel nonlinearity is kept in the simulation. This results are consistent with the nonlinear gyrokinetic theory for the GAM, which shows that the perpendicular convective nonlinearity can be cancelled by the parallel nonlinearity in the long wavelength limit ($k_r\rho_i \ll 1$, where k_r is the GAM radial wavelength and ρ_i is the ion gyroradius). GTC has been successfully applied to the simulations of MHD modes such as TAE[9] and RSAE[10]. In the BAE study[11], we successfully excite the BAE in GTC simulations both through an

external antenna and by energetic particle density gradients. The antenna excitation enables us to measure the BAE frequency, damping rate and mode structure accurately. We find that the BAE frequency at small q is slightly higher than the BAE accumulation point frequency, and also higher than the theoretical prediction. In the energetic particle excitation, the non-perturbative contributions by energetic particles modify the BAE mode structure and frequency relative to ideal MHD theory. The finite Larmor radius effects of energetic particles reduces the BAE growth rate. We note that GTC simulation of BAE is the first global gyrokinetic simulation of BAE. GTC gyrokinetic simulation has been successfully benchmarked with an extended hybrid-MHD gyrokinetic code XHMGC[12].

2. GAM collisionless damping by trapped electrons

In our GTC particle simulations, a flux-surface-averaged ion guiding center density perturbation is initiated to generate the GAM. The radial profile of the GAM is set to be a $\sin$ function with the wavevector to be $k_r\rho_i = 0.11$. And the density perturbation at the inner and outer boundary is initiated to be zero. We use a small simulation domain $\Delta r = [0.45a, 0.55a]$ (a is the minor radius), $T_i = T_e$, and a constant q profile as the magnetic shear has little effect on the GAM damping. An electrostatic version of the fluid-kinetic hybrid electron model[13, 14] is used to treat the kinetic electron response in our simulations.

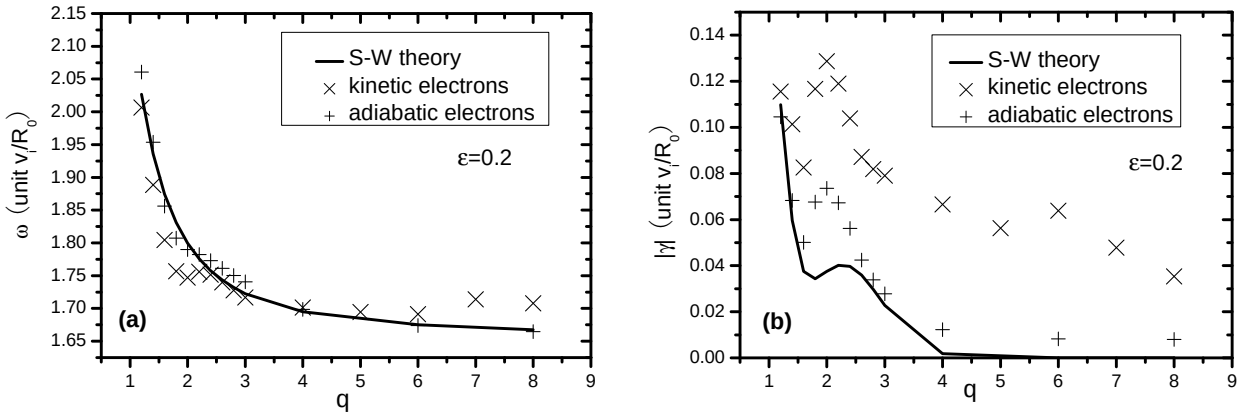

Figure 1: *Comparison of the GAM real frequency and damping rate between adiabatic and kinetic electron simulations at different q.*

In the simulation with adiabatic electron response, the GAM real frequency and damping rate agree with Sugama and Watanabe's theory (S-W theory) very well in the theory's limit[7, 15]. Since the number of trapped particles is proportional to $\sqrt{\epsilon}$, $\epsilon = 0.2$ is used in the simulations with kinetic electron response and comparisons are made between kinetic and adiabatic electron simulations. It is shown that the GAM frequency is insensitive to the trapped electrons while the GAM damping rate is significantly enhanced (Fig. 1). From Fig. 1 (a), the frequency of the simulations with kinetic electrons also agrees with the S-W theory. As for the damping rate in Fig. 1 (b), simulation results with adiabatic electrons at $\epsilon = 0.2$ is slightly higher than the theory due to the finite ϵ effects[16]. More importantly, we find that the damping rate in the simulations with kinetic electrons at $\epsilon = 0.2$ is much higher than that of adiabatic

electrons. We note that when q is larger than 3.0, the results of simulation with kinetic electrons are almost one order of magnitude higher than adiabatic electrons. This means that the trapped electron effect is typically more important than the finite orbit width effect on the GAM damping rate in the high-q region.

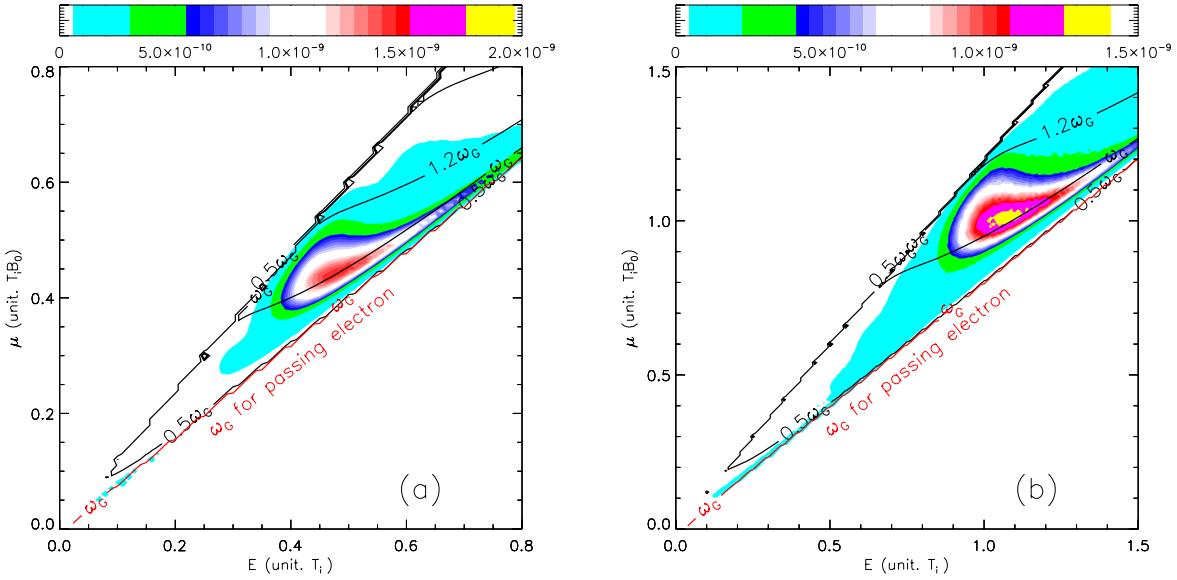

Figure 2: *Contour plot of trapped electron bounce frequency ω_{be} and passing electron transit frequency ω_{te} (in unit of $\omega_{_G} \equiv \omega_{_{GAM}}$) along with the simulation result of the $(\delta f_e/f_{e0})^2$ in $E-\mu$ space. Here (a) and (b) are simulation with $q=4$ and $q=6$, respectively.*

In order to further illustrate that the enhancement of the GAM damping rate in the kinetic electron simulation is mainly due to the trapped electron response, we analyze the $(\delta f_e/f_{eo})^2$ in $E-\mu$ phase space (δf_e is the electron density perturbation, E and μ are the electron energy and magnetic moment, respectively). The initial δf_e is set to be zero, while the ion guiding center density perturbation is initiated as a flux-surface-averaged quantity. If trapped electron bounce motion resonates with GAM oscillation, the amplitude of $(\delta f_e/f_{e0})^2$ for the resonant electrons in the phase space will increase faster than the non-resonant electrons. As electron bounce frequency is only the function of E and μ, we plot the electron bounce frequency along with the $(\delta f_e/f_{e0})^2$ in the same $E-\mu$ phase space (Fig. 2). The electron bounce frequency is integrated by the following equation:

$$\omega_{be} = 2\pi/\tau_{be} = 2\pi\left(\int_{-\theta_b}^{\theta_b} \frac{dl}{|v_{||}|}\right)^{-1} = 2\pi\left(\int_{-\theta_b}^{\theta_b} \frac{dl}{\sqrt{2(E-\mu B)}}\right)^{-1}. \quad (1)$$

Here τ_{be} and θ_b is the trapped electron bounce period and poloidal angle at the turning point, respectively. From Fig. 2 we can see that the $(\delta f_e/f_{e0})^2$ of the trapped electrons with bounce frequency around the GAM frequency $\omega_{_{GAM}} = \omega_{be}$ is much larger than that of other trapped electrons. Comparing Fig. 2 (a) and (b), we can see that the maximum of $(\delta f_e/f_{e0})^2$ locates at $E \approx 0.45(T_i)$ and $E \approx 1.0(T_i)$ for $q = 4.0$ and $q = 6.0$, respectively. It also agrees with the bounce frequency relation $\omega_{be} \propto \sqrt{T_i}/q$ for deeply trapped electrons. These simulation

results clearly show that the enhancement of the GAM damping rate in simulations with kinetic electrons is due to the resonance between the GAM oscillation and the trapped electron bounce motion.

3. Importance of parallel nonlinearity in GAM nonlinear self-interaction

In the D-IIID experiment[17], the nonlinear generation of the second harmonic of GAM has been observed. The detected GAM density fluctuation near the mid-plane is around $1-2\%$ and the extrapolated peak fluctuation is $10-15\%$. In our simulations, the D-IIID experiment parameters are used as much as possible. The parallel nonlinearity are not included first. We use an initial perturbation of the ion guiding center density $\delta n_{00}/n_0 = 0.01$. The density perturbation $\delta n_{01}/n_0$ is initially zero, but rises within a GAM oscillation period to a value of $\delta n_{01}/n_0 \approx 0.1$. The second harmonic with a characteristic frequency of $2\omega_{_{GAM}}$ is observed in this nonlinear regime as we can see from Fig. 3 (a). A zero-frequency density perturbation components is also excited. This indicates that when GAM amplitude grows large enough, a three-wave interaction process occurs: GAM couples with itself and produces two branches of daughter waves i.e. a zero-frequency component and the second harmonic component. Next, we include the parallel nonlinearity and keep other parameters the same to perform the simulation. Figure 3 (b) shows that the parallel nonlinearity obviously suppresses the generation of the second harmonic in large amplitude GAM simulation. This result can be easily understood from the nonlinear gyrokinetic theory[8].

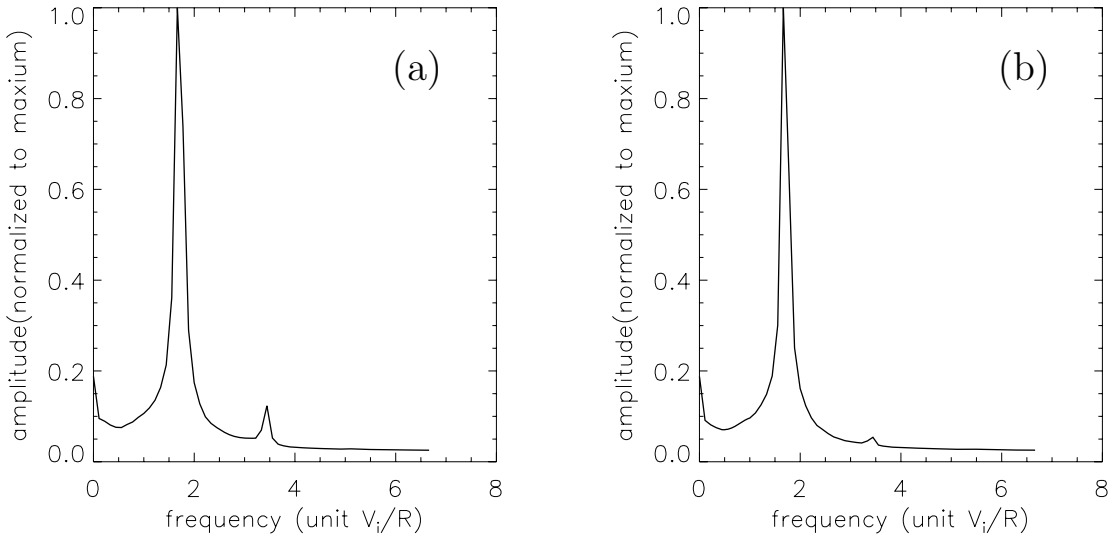

Figure 3: *Frequency spectrum of δn_0 in large amplitude GAM simulations without parallel nonlinearity (a) and with parallel nonlinearity (b).*

Beginning from the nonlinear gyrokinetic equation[18], the GAM second harmonic generation can be written as:

$$(\frac{\partial}{\partial t} + i\omega_d)\delta F^{II} + \delta\dot{\mathbf{X}}^I \cdot \frac{\partial}{\partial \mathbf{X}}\delta F^I + \delta\dot{W}^I \frac{\partial}{\partial W}\delta F^I = 0, \tag{2}$$

in which, $F = F(\mathbf{Z}, t)$, $\mathbf{Z} = (\mathbf{X}, W, \mu)$ is the five-dimensional gyrocenter phase space with $\mathbf{X}$, W and μ being the gyrocenter position, the parallel velocity, and the magnetic moment, respectively. $\omega_d = \hat{\omega}_d \sin\theta = -k_r m_i (v_\perp^2/2 + v_\parallel^2)\sin\theta/(eBR)$ is the magnetic drift associated with the geodesic curvature, the superscripts I and II represent the primary and the second harmonic, respectively. Here, we consider only the lowest order nonlinear effects, thus we ignore the $O(\omega_d/\omega) \approx O(k_r\rho_i)$ term. For the electrostatic case, we have:

$$\delta\dot{\mathbf{X}}^I = \frac{1}{B}\hat{\mathbf{b}} \times \nabla\langle\delta\phi^I\rangle, \tag{3}$$

$$\delta\dot{W}^I = -\frac{e}{m}\hat{\mathbf{b}} \cdot \nabla\langle\delta\phi^I\rangle - \frac{1}{B}\nabla \times (W\hat{\mathbf{b}}) \cdot \nabla\langle\delta\phi^I\rangle. \tag{4}$$

We note that in Eq.(2), the second term is the usual perpendicular nonlinear convective term, and is given by:

$$\delta F_{nl,R}^{II} = -\frac{e^2 k_r^I}{m\Omega T_i r}\frac{\hat{\omega}_d}{\omega^I\omega^{II}} F_0 \cos\theta (\delta\phi_{00}^I)^2. \tag{5}$$

The last term is the parallel nonlinear term. If we neglect this term, the ratio between the amplitude of the second and primary harmonic of GAM is thus, given by:

$$\left|\frac{\delta E_r^{II}}{\delta E_r^I}\right| = A\frac{\delta E_r^I}{B v_i}; \quad \text{where} \quad A = \frac{1}{6Sk_r^I\rho_i}. \tag{6}$$

In our simulations with $k_r^I\rho_i = 0.1$ and $S = 2.9$, we get $A = 0.58$, which is in reasonable agreement with the numerical fitting of the GTC simulation result $A \approx 0.95$. By considering the parallel nonlinearity term, it gives

$$\delta F_{nl,P}^{II} = \frac{e^2 k_r^I}{m\Omega T_i R}\frac{\hat{\omega_d^I}}{\omega^I\omega^{II}} F_0 \sin^2\theta (\delta\phi_{00}^I)^2. \tag{7}$$

This term will cancel exactly the perpendicular nonlinear convective term after surface average. So the nonlinear harmonic generation of GAM, is higher order in $O(\omega_d/\omega) \approx O(k_r\rho_i)$ effect than the parallel nonlinearity term, and is thus, ignorable.

4. BAE excitation by antenna and energetic particles

In this simulation, we use $a/R_0 = 0.3$ (a and R_0 are tokamak the minor and major radius, respectively.). Protons are used as the background ions while electron temperature is $T_e = 0$. In this case, the Aflvén accumulation point frequency is $\omega_{BAE} = \sqrt{(7/4)T_i/(m_i R_0^2)} \approx 1.32 v_i/R_0$. The background plasma is uniform with $\beta = 4\pi n_0(T_i + T_e)/B_0^2 = 0.0072$. The $q = 2$ mode rational surface locates at $\epsilon = r/R_0 = 0.15$ (r is the local minor radius). The $n = 4$ mode is selected in the linear simulation. Since the BAE is a $k_\parallel \approx 0$ mode, we additionally apply a poloidal filter to keep only the $m = nq$ and $m = nq \pm 1$ harmonics to avoid the high frequency noise. The wavelength of the BAE is $k_\theta\rho_i = 0.09$.

First, an external antenna is used to excite the BAE. Finite Larmor radius effects are ignored. Figure 4 (a) is the time evolution of the $(n = 4, m = 8)$ BAE mode excited with an antenna frequency $\omega_{ant} = 1.67 v_i/R_0$. The mode amplitude saturates quickly due to the large damping rate. Figure 4 (b) is the poloidal mode structure of the electrostatic potential. The $m = 8$ harmonic is well formed around the $q = 2$ mode rational surface. According to the resonant

theory, if a damped eigenmode is excited by an antenna, the saturated intensity of the eigenmode is given by:

$$A^2 \propto \frac{1}{(\omega_0^2 + \gamma^2 - \omega_{ant}^2)^2 + 4\gamma^2\omega_{ant}^2} \tag{8}$$

Here, A^2 is the normalized saturated intensity. ω_0 and γ are the real frequency and damping rate of the eigenmode, respectively. This method is also used in tokamak experiments to measure the mode frequency and damping rate[19]. Figure 4 (c) is the antenna frequency scan of the saturated BAE amplitude. The numerical fitting of the simulation results by Eq. 8 shows that the eigen frequency and damping rate are $1.65v_i/R_0$ and $-0.36v_i/R_0$, respectively. The observed frequency is about 25% higher than ω_{BAE} and also about 15% higher than the theoretical prediction in Refs [20, 21, 22]. We note that these theories are based on the assumption of small ϵ and large q. The large damping rate suggests that the ion Landau damping effect is strong, because the BAE frequency is close to the thermal ion transit frequency $\omega_t = v_i/(qR_0)$.

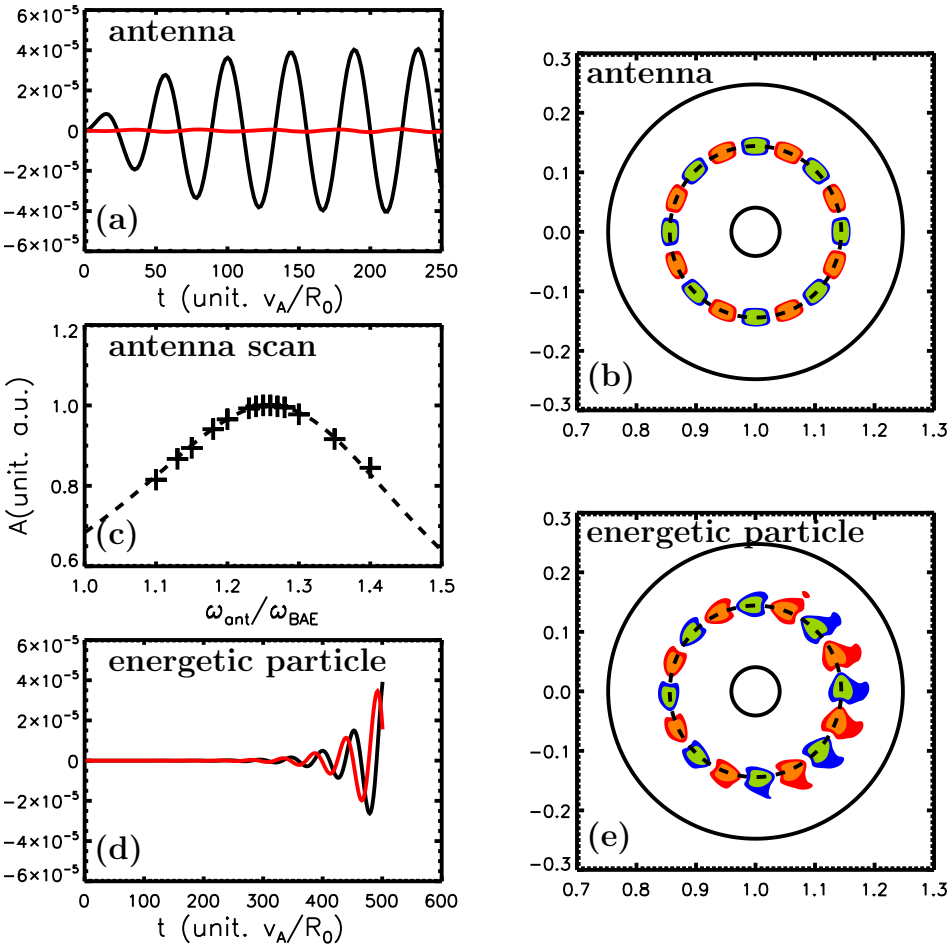

Figure 4: *Time evolution (panel (a)) and poloidal mode structure (panel (b)) of the BAE excited by antenna with $\omega_{ant} = 1.67v_i/R_0$. Panel (c): saturated amplitude vs antenna frequency. The dash line is the numerical fitting by Eq. 8. Panels (d) and (e) are the time evolution and poloidal mode structure of the BAE excited by energetic particles. In panels (a) and (d), the black line is the real part and the red line is the imaginary part. In panels (b) and (e), the dash circle is the $q = 2$ mode rational surface.*

Next, the energetic particle density gradient is used to excite the BAE. We also use protons as the energetic particles. The maximum density gradient $R/L_{nf} \approx 46$ is located at the $q = 2$ and $\epsilon = 0.15$ surface. The energetic particles have a Maxwellian distribution with $T_f = 16T_i$ and $n_f = 0.01n_0$, respectively. In this case, the energetic particle diamagnetic frequency is $\omega_{*f} \approx 47v_i/R_0$ and $k_\theta \rho_E = 0.36$. The drift-kinetic limit is taken first for simplicity and for comparison with the gyrokinetic simulation with finite Larmor radius effects. Figure 4 (d) is the time evolution of the BAE mode. Different from Fig. 4 (a), the energetic particle excited BAE mode grows exponentially. The imaginary part of the mode is $\pi/2$ leading the real part in phase, which means that this wave is a traveling wave and propagates in the fast ion diamagnetic direction. The mode frequency and growth rate are $1.40v_i/R_0$ and $0.25v_i/R_0$, respectively. The frequency is slightly lower than the antenna result due to the non-perturbative contribution by energetic particles. The gyrokinetic simulation with finite Larmor radius effects is also carried out with the same parameters, and the frequency and growth rate are $1.44v_i/R_0$ and $0.19v_i/R_0$, respectively. The difference between the gyrokinetic and the drift-kinetic simulations for the BAE linear growth rate is due to finite Larmor radius effects. Comparing the poloidal mode structure of the antenna excitation case (Fig. 4 (b)) and the energetic particle excitation case (Fig. 4 (e)), the mode structure in Fig. 4 (b) is slightly different from Fig. 4 (e), since the energetic particles are treated non-perturbatively, which break the radial symmetry. This work is the first gyrokinetic particle simulation of the BAE, benchmarks between gyrokinetic particle simulation and hybrid-MHD simulation are carried out and show good agreement in BAE frequency and mode structure[11].

5. Conclusion

In this work, we use gyrokinetic particle simulation to study the GAM collisionless damping, nonlinear self-interaction and BAE excitation in toroidal plasmas. Our simulation results show that the GAM frequency is insensitive to the kinetic electrons but the GAM damping rate is greatly enhanced. The enhancement of the GAM collisionless damping rate is due to the resonance of trapped electron bounce motion with the GAM oscillation. This result provides a possible explanation of the finite GAM damping rate in the high-q region of the tokamak edge, where the contribution of the ion resonance is small.

Nonlinear self-interactions of the GAM cannot efficiently generate the second harmonic due to a cancellation between the perpendicular convective nonlinearity and the parallel nonlinearity for the long wavelength GAM. Other mechanisms are required to explain recent experimental observations of the excitation of the GAM second harmonic.

In the BAE excitation simulation, the BAE frequency in antenna excitation is slightly higher than the MHD accumulation point frequency due to the thermal ion kinetic effects. In the BAE simulation of energetic particle excitation, the frequency is reduced and the mode structure is modified by the non-perturbative contributions of the energetic particles. The BAE growth rate can also be reduced by the finite Larmor radius effect.

Acknowledgment

This work was supported by the U. S. Department of Energy (DOE) SciDAC GSEP and GPS centers, the China Scholarship Council (Grant No. 2009601135) and National Basic Research Program of China (Grant No. 2008CB717803 and 2009GB105000).

References

[1] N. Winsor, J. L. Johnson and J. J. Dawson, *Phys. Fluids* **11**, 2448 (1968).

[2] W. W. Heidbrink et al, *Phy. Rev. Lett.* **71**, 855 (1993).

[3] A. Fujisawa, *Nucl. Fusion* **49**, 013001 (2009).

[4] W. W. Heidbrink et al, *Phys. Plasmas* **6**, 1147 (1999).

[5] Z. Lin et al, *Science* **281**, 1835 (1998).

[6] I. Holod et al, *Phys. Plasmas* **16** 122307 (2009).

[7] H. S. Zhang and Z. Lin, *Phys. Plasmas* **17** 072502 (2010).

[8] H. S. Zhang et al, *Nucl. Fusion* **49** 125009 (2009).

[9] Y. Nishimura, *Phys. Plasmas* **16**, 030702 (2009).

[10] W. J. Deng et al, *Gyrokinetic particle simulations of reversed shear Alfvén eigenmode excited by antenna and fast ions*, *Phys. Plasmas* (2010) in press.

[11] H. S. Zhang, Z. Lin, *Gyrokinetic particle simulation of beta-induced Alfvén eigenmode*, *Phys. Plasmas* (2010) in press.

[12] X. Wang et al, 23^{rd} *IAEA Fusion Energy Conf.* (2010).

[13] Z. Lin and L. Chen, *Phys. Plasmas* **8**, 1447 (2001).

[14] Z. Lin et al, *Plasma Phys. Control. Fusion* **49**, B163 (2007).

[15] H. Sugama and T. H. Watanabe, *J. Plasma Physics* **72**, 825 (2006).

[16] X. Q. Xu et al, *Phys. Rev. Lett.* **100**, 215001 (2008).

[17] R. Nazikian et al *Phys. Rev. Lett.* **101**, 185001 (2008).

[18] A. J. Brizard, *Phy. Plasmas* **2**, 459 (1995).

[19] A. Fasoli et al, *Phy. Rev. Lett.* **75**, 645 (1995).

[20] C. Nguyen, X. Garbet and A. I. Smolyakov, *Phys. Plasmas* **15**, 115002 (2008).

[21] A. I. Smolyakov, C. Nguyen and X. Garbet *Nucl. Fusion* **50**, 054002 (2010).

[22] X. Wang, F. Zonca, and L. Chen, *Theory and simulation of discrete kinetic beta-induced Alfvén eigenmode in tokamak plasmas*, *Plasma Phys. Controlled Fusion* (2010) in press.